

Inhibition-Induced Theta Resonance in Cortical Circuits

Eran Stark,^{1,*} Ronny Eichler,¹ Lisa Roux,¹ Shigeyoshi Fujisawa,¹ Horacio G. Rotstein,² and György Buzsáki^{1,*}

¹NYU Neuroscience Institute, School of Medicine, New York University, New York, NY 10016, USA

²Department of Mathematical Sciences, New Jersey Institute of Technology, Newark, NJ 07102, USA

*Correspondence: eranstark@gmail.com (E.S.), gyorgy.buzsaki@nyumc.org (G.B.)

<http://dx.doi.org/10.1016/j.neuron.2013.09.033>

SUMMARY

Both circuit and single-cell properties contribute to network rhythms. In vitro, pyramidal cells exhibit theta-band membrane potential (subthreshold) resonance, but whether and how subthreshold resonance translates into spiking resonance in freely behaving animals is unknown. Here, we used optogenetic activation to trigger spiking in pyramidal cells or parvalbumin immunoreactive interneurons (PV) in the hippocampus and neocortex of freely behaving rodents. Individual directly activated pyramidal cells exhibited narrow-band spiking centered on a wide range of frequencies. In contrast, PV photoactivation indirectly induced theta-band-limited, excess post-inhibitory spiking in pyramidal cells (resonance). PV-inhibited pyramidal cells and interneurons spiked at PV-inhibition troughs, similar to CA1 cells during spontaneous theta oscillations. Pharmacological blockade of hyperpolarization-activated (I_h) currents abolished theta resonance. Inhibition-induced theta-band spiking was replicated in a pyramidal cell-interneuron model that included I_h . Thus, PV interneurons mediate pyramidal cell spiking resonance in intact cortical networks, favoring transmission at theta frequency.

INTRODUCTION

Theta (4–11 Hz) oscillations provide a basis for temporal coding of spatial information and episodic memory in the hippocampus (O'Keefe and Recce, 1993; Buzsáki and Moser, 2013). The theta rhythm is generated by a consortium of mechanisms, including a septal pacemaker, circuit interactions, and intrinsic properties of single neurons (Buzsáki, 2002). A potentially important mechanism contributing to theta generation is the resonant properties of neurons (Leung and Yu, 1998; Dickson et al., 2000; Pike et al., 2000; Haas and White, 2002; Hu et al., 2002; Erchova et al., 2004; Lengyel et al., 2005; Giocomo et al., 2007; Gastrein et al., 2011). In general, resonance refers to an amplifying mechanism in a limited frequency band (Hutcheon and Yarom, 2000). In vitro, intracellular sinusoidal current injection into hippocampal pyramidal neurons yields subthreshold membrane potential oscilla-

tions with a maximum amplitude in the theta band (Leung and Yu, 1998; Pike et al., 2000; Hu et al., 2002; Zemankovics et al., 2010). Subthreshold theta-band resonance is largely mediated by the hyperpolarization-activated cyclic nucleotide-sensitive (HCN) channels, which generate a nonselective cation current, I_h (Gasparini and DiFrancesco, 1997; Robinson and Siegelbaum, 2003). HCN1 channels are especially abundant in the distal apical dendrites of CA1 and neocortical layer 5 pyramidal cells (Magee 1998; Stuart and Spruston, 1998; Santoro et al., 2000; Lörincz et al., 2002; Ulrich, 2002). The inductive effects of I_h create a negative feedback that opposes the voltage changes and thus creates resonance (Narayanan and Johnston, 2008). Because HCN1 channels are active at a hyperpolarized membrane potential, theta resonance in circuits is expected to depend on interaction between inhibitory interneurons and pyramidal cells. Indeed, theta-frequency burst discharge of hippocampal basket cells can effectively coordinate spike timing of target pyramidal neurons and induce rebound spikes after release from hyperpolarization in vitro (Cobb et al., 1995). Yet, it is not clear if and how subthreshold resonance is translated to the suprathreshold (spiking) regime (Magee, 1998; Pike et al., 2000; Ulrich, 2002; Richardson et al., 2003) in behaving animals.

Subsets of neurons in the neocortex can also phase-lock to hippocampal theta oscillations (Siapas et al., 2005; Sirota et al., 2008), possibly entrained by interneurons, but it is unknown whether resonance-related mechanisms are involved in this process. More generally, it remains to be demonstrated whether neuronal spiking and interneuronal information transfer are sensitive to input at any specific frequency range. To determine the importance of input frequency for spiking activity in the intact hippocampus and neocortex, we examined spiking responses of pyramidal cells and interneurons to optogenetically induced membrane potential oscillations at various frequencies in freely behaving animals. Light activation was confined to a small group of nearby neurons (Stark et al., 2012) so that the cellular-synaptic mechanisms could be investigated without altering the network state or the oscillatory frequency/phase of native rhythms.

RESULTS

Pyramidal Cells Spike Preferentially in the Theta Band during Light-Induced PV Cell Activation

For cell type-specific control of neuronal spiking, mice expressing ChR2 (Boyden et al., 2005) either in pyramidal neurons

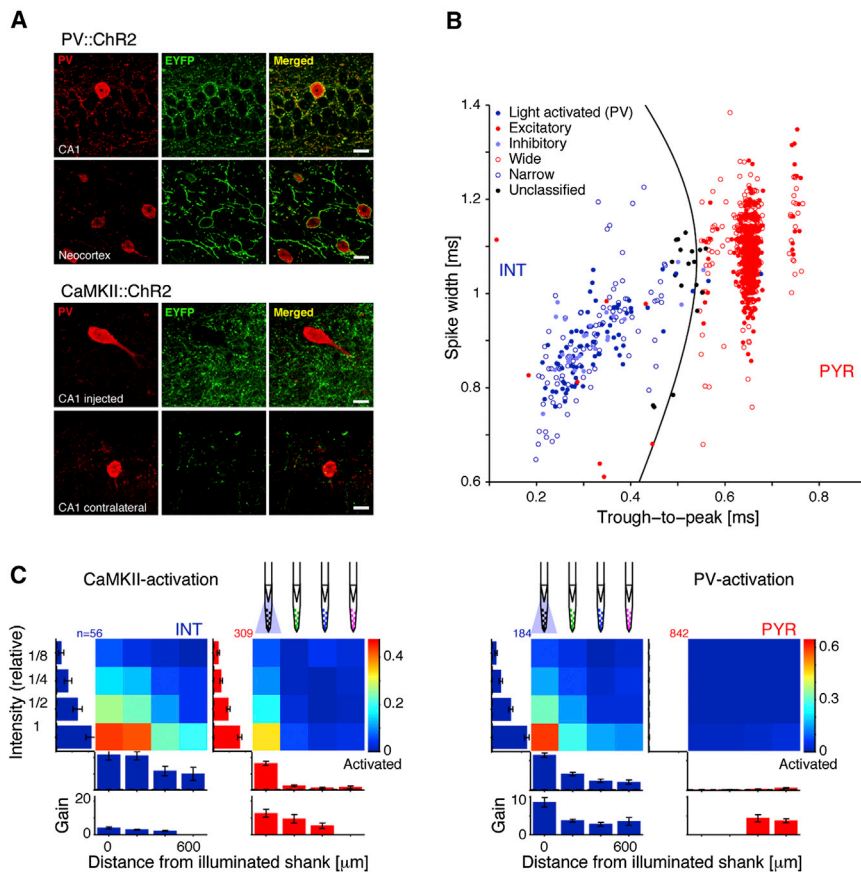


Figure 1. Local Activation of Specific Cell Types in Freely Moving Mice

(A) Immunostaining for PV colocalizes with EYFP, the reporter gene for ChR2 expression, in PV-cre::Ai32 mice but not in animals injected unilaterally with rAAV5/CamKIIa-hChR2(h134R)-EYFP viruses. In five PV-cre::Ai32 animals, all 84 EYFP+ cells were PV+ (100%) and 84 of 93 PV+ cells were EYFP+ (90%). Calibration, 15 μm.

(B) Units are tagged as excitatory or inhibitory based on monosynaptic peaks/troughs in the cross-correlation histogram ($p < 0.001$, convolution method; Stark and Abeles, 2009) and/or locally delivered 50–70 ms light pulses ($p < 0.001$, Poisson test; PV animals only). Nontagged units (692 of 1,413, 51%) are classified as putative pyramidal cells (PYR) or interneurons (INT) according to waveform morphology; nontagged units with low classification confidence ($p > 0.05$, $n = 22$, 1.6%) are not analyzed (“unclassified”).

(C) Effect of single-shank pulses on locally recorded and distant cells ($\geq 200 \mu\text{m}$; $n = 4$ CaMKII mice, 8 PV mice). Intensities are scaled by the level used to induce the largest number of directly activated units per shank (the “optimal” DC intensity). Mean intensities at the center of the illuminated shanks were 0.56 (CaMKII) and 1.1 mW/mm² (PV). Bars below are group means (SEM) for the optimal intensity, and bars at the left refer to the local shank. CaMKII activation induces local spiking of PYR at a higher gain (bottom; defined as the firing rate during DC pulses divided by baseline firing rate, in the lack of light) than INT, whereas PV activation induces only localized INT spiking. See also Figure S1.

(CaMKII::ChR2; $n = 4$ mice) or in the parvalbumin class of inhibitory interneurons (PV::ChR2; $n = 8$ mice) were used (Figure 1A). Animals were chronically implanted with multishank diode probes that enable independent light stimulation of small local groups of neurons while concurrently recording the extracellular spiking activity of directly and indirectly activated cells (Stark et al., 2012). Cells were classified as putative pyramidal cells (PYR) or interneurons based on monosynaptic connectivity, an increase in spiking during brief light pulses, and/or spike waveform features (Figure 1B, Figure S1 available online). Single-shank photostimulation with direct current (DC) pulses (50–70 ms) resulted in localized activation of targeted cells. At the “optimal” intensity (activating the largest number of targeted units per shank), 33% (101/309) of locally stimulated PYR were activated ($p < 0.05$; Poisson test) in CaMKII::ChR2 mice, whereas in PV::ChR2 animals, 59% (108/184) of locally stimulated interneurons were activated (Figure 1C) and these are referred to as PV cells throughout this paper. The abbreviation INT refers to physiologically identified putative interneurons that were not driven during PV photostimulation (a subset of INT may be PV cells that were not activated by light). Other (nonlocal and/or nontargeted) cells were weakly activated (e.g., INT recorded in CaMKII::ChR2 mice; Figure 1C, left) or not activated (e.g., local PYR recorded in PV::ChR2; Figure 1C, right). These findings illustrate effective spatiotemporal control of specific cell types in freely moving mice.

Selective stimulation of PYR with a time-varying chirp pattern (linear 0–40 Hz, 10 s; Figure 2A, bottom) induced spiking ($p < 0.05$; permutation test) at various frequencies with similar probabilities ($p = 0.41$, χ^2 test) in single PYR (121/257, 47%) and INT (27/46, 59%) in both hippocampus and neocortex (Figures 2A and 2C, left). Neurons typically spiked near the stimulus peak (at maximum light intensity/zero phase; Figure 2C, left; Figure S2A) but with slight phase shifts at progressively higher frequencies of the chirp (Figure 2C, bottom left; PYR: linear model, $\Phi(f) = -0.1 + 0.03f$; mean R^2 over $n = 121$ cells: 0.7; INT: $\Phi(f) = 0.29 + 0.02f$; $R^2 = 0.57$, $n = 27$; Figure 2D; Figure S2). Thus, PYR preceded INT spiking with a frequency-dependent delay, which was likely brought about by the kinetics of ChR2 (Boyden et al., 2005) and/or differential spike-generating mechanisms. Although individual PYR tended to spike at narrow frequency bands, this band differed from cell to cell and, at the group level, spanned the entire range of tested frequencies ($p = 0.44$; Kolmogorov-Smirnov test with a uniform null; Figure 2C, left; Figure S2B).

Chirp-pattern photostimulation of PV interneurons often induced high firing rates (mean \pm SEM 142 ± 13 spikes/sec, $n = 52$ frequency modulated PV; Figure S2D) and wide-band spiking in these directly stimulated cells (Figure 2Bd), compared with just one or two spikes per cycle typically emitted during direct PYR stimulation (compare the left and right traces in Figure 2A). Overall, 60% of the tested interneurons (52/86) showed

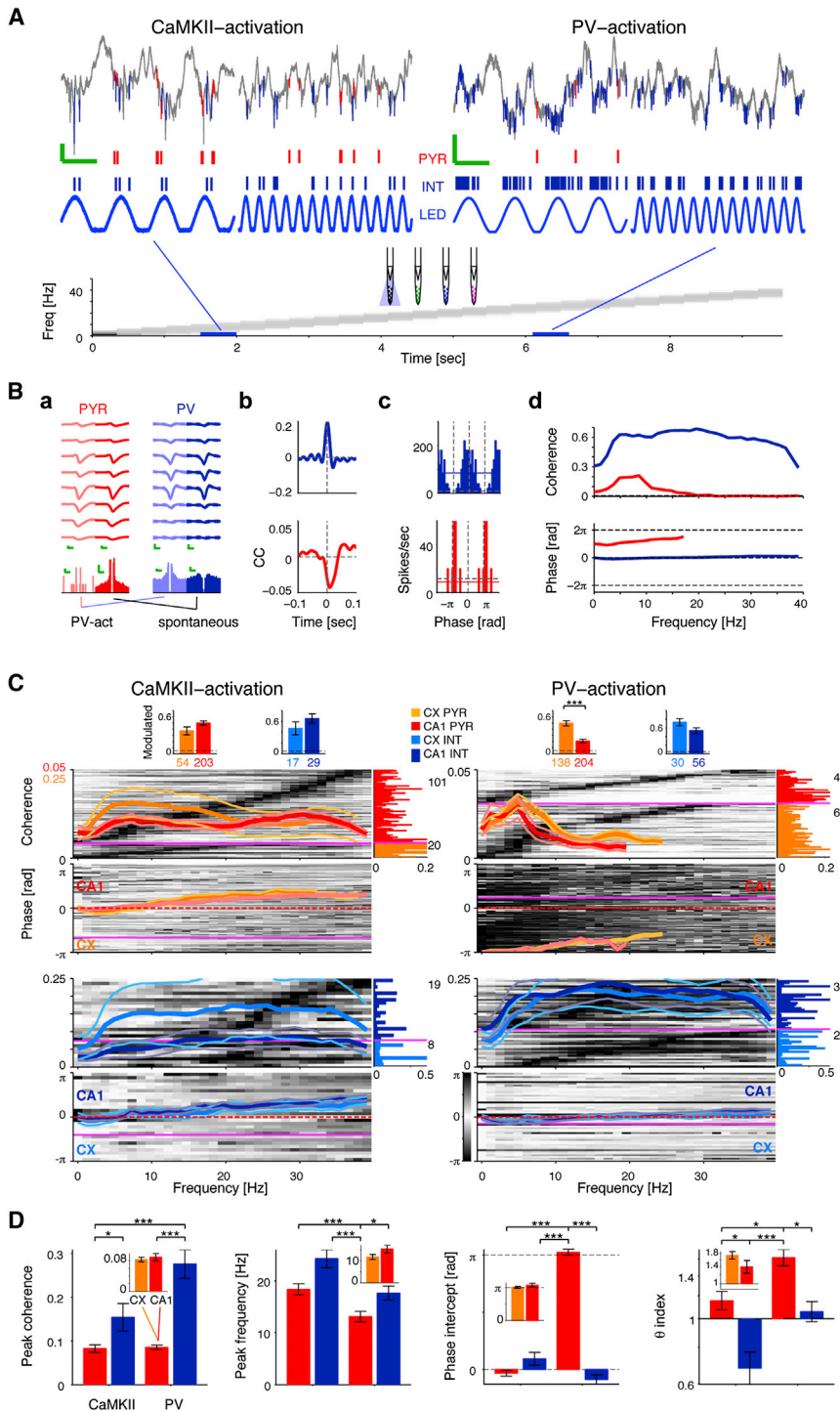


Figure 2. Band-Limited Spiking of Pyramidal Cells Is Centered at Theta by Inhibition

(A) Example traces of local field potentials (LFP) and spikes (1–5,000 Hz; calibration: 100 ms, 200 μ V) in the CA1 pyramidal layer during chirp pattern photostimulation (0–40 Hz gray ramp; peak 470 nm light intensity, approximately 0.9 mW/mm² at shank center) of PYR (CaMKII, left) or PV-interneurons (PV, right). During CaMKII-activation, cells spike at a broad range of frequencies, whereas during PV-activation, PYR tend to spike specifically at theta frequency.

(B) Example analysis for the CA1 PYR-PV pair during PV-activation. (Ba) Waveforms of the pyramidal cell (PYR) and interneuron (PV) at the eight sites of the diode-probe shank (20 μ m spacing) during PV activation and spontaneous activity (mean and SD; calibration: 0.25 ms, 50 μ V). Calibration for autocorrelation histograms: 10 ms, 10 spikes/s. (Bb) Time-domain cross-correlation between the chirp pattern and spiking activity (both sampled at 1,250 Hz). While the PV cell is activated, PYR spiking is largely suppressed (note difference in scale). (Bc) Theta phase histograms for all spikes, expressed as firing rates (20 phase bins/cycle); horizontal dashed lines show baseline rates (mean over all periods without light stimulation) and continuous colored lines show mean firing rate during the theta (6 \pm 1 Hz) chirp segment. Phase 0 corresponds to stimulus peak. (Bd) Coherence (top) and phase (bottom) between chirp pattern and spiking; dashed line shows chance coherence; phase is shown only for frequencies in which coherence is significant ($p < 0.05$, Bonferroni-corrected permutation test). During theta-band chirp pattern PV activation (red), the PYR spikes specifically at chirp troughs.

(C) Spiking activity of neocortical (CX) and CA1 cells during PYR (left) or PV (right) photostimulation (0–40 Hz chirp pattern). Coherence (scaled 0–1; peak values shown at right) and phase plots for all neurons (rows) and group mean \pm SEM are shown. Bars at right show peak coherence for each cell; proportions of cells modulated by the chirp pattern ($p < 0.05$, permutation test) are shown at top. Spike phases are near zero with a linear shift for both cell types during CaMKII stimulation (left) and for PV interneurons during PV stimulation (right). Note narrow-band coherence of individual PYR at a wide range of frequencies during CaMKII activation but predominant theta band-limited coherence during PV activation.

(D) Statistical analysis of various measures for PYR (red) and INT (blue). Insets show comparisons between neocortical (orange) and CA1 (red) PYR during PV activation. Color code is the same for in all panels. Error bars, SEM; */**/** $p < 0.05/0.01/0.005$, Kruskal-Wallis test, Bonferroni-corrected for multiple comparisons. θ index is defined as theta band (4–11 Hz) coherence, divided by the overall mean coherence (0–40 Hz). Peak coherence frequency, phase intercept, and theta preference of PYR depend on the activated cell type. See also Figure S2.

significant coherence between the chirp and spiking ($p < 0.05$, permutation test; Figure 2C, top right) with increasing phase shifts at higher frequencies ($\Phi(f) = -0.27 + 0.016f$; $R^2 = 0.7$; Figure 2D). In contrast, PV stimulation induced band-limited spiking in PYR (110/342, 32%; Figures 2Bd and 2C, top right), confined

mainly to the trough of the stimulus (Figure 2Bc; Figure 2D, right; $\Phi(f) = (\pi + 0.08) + 0.03f$; $R^2 = 0.7$). The significant coherence between the light stimulus and spiking was predominantly at the theta frequency band (4–11 Hz; Figure 2C, top right; $p < 0.001$, Kolmogorov-Smirnov test with a uniform null; Figure S2B).

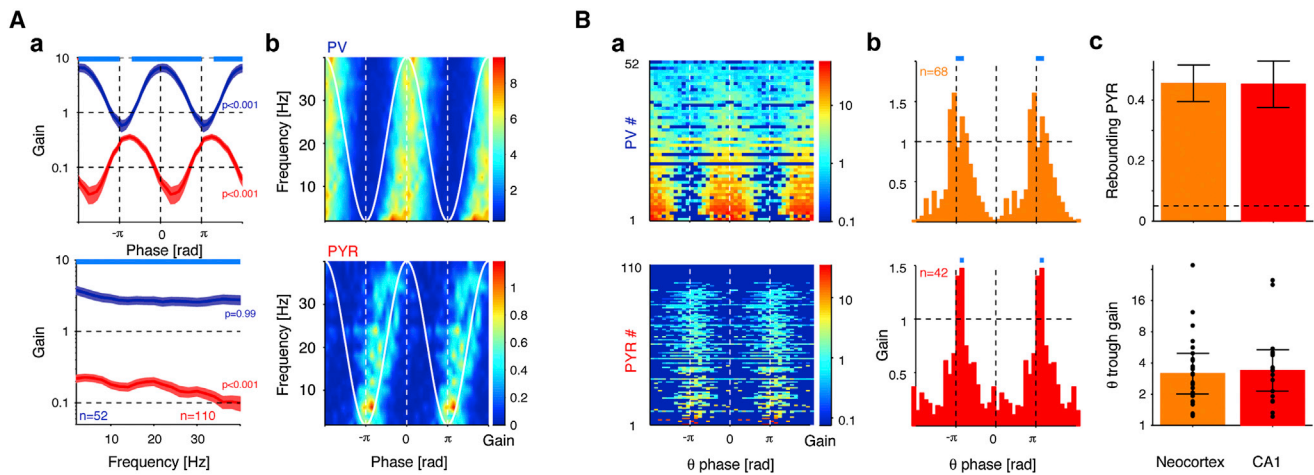


Figure 3. Inhibition Induces Excess Spiking of Pyramidal Cells

(A) Spiking gain during PV-activation. (Aa) For each cell, firing rates resolved by chirp phase (top) or chirp frequency (bottom) were computed and divided by the baseline rate (in the lack of any light stimulation). Gain = 1 thus indicates no change relative to spontaneous activity. Error bands, SEM; light blue bars, phases (or frequencies) for which PYR and PV gain differ ($p < 0.01$, Bonferroni-corrected Kruskal-Wallis test). PYR spiking is suppressed at all phases (when averaged over all frequencies) and frequencies (when averaging over all phases). (Ab) Gain plotted as a frequency-phase map (bin size: 2 Hz, $\pi/10$ rad). PV interneurons spike around chirp peaks (0 radians) at all frequencies; the peak average gain for PV is at 6–8 Hz, just after the chirp trough.

(B) Theta (4–11 Hz) gain of individual PV interneurons (top) and PYR (bottom; Ba). Units are sorted by the maximum gain; some light-driven units do not spike in the theta band of the chirp. (Bb) Mean theta gain for the PYR, partitioned by brain region. Blue bars indicate phase bins for which the number of units with increased spiking (gain > 1) exceeds chance level (exact Binomial test, $p < 0.001$). In both brain regions, the mean gain is > 1 at the chirp theta trough. (Bc) Top, the fractions of PYR exhibiting excess (“rebound”) spiking, defined as units with increased spiking during troughs of theta-band chirp, are similar in neocortex and CA1 ($p = 0.97$, χ^2 test). Bottom, gain (median \pm median average deviation) of rebounding PYR in neocortex and CA1 is similar ($p = 0.91$, U test). Dots, gain of individual PYR. For more details, see Figure S3.

To quantify theta-band preference, we calculated a “theta index” for each cell (mean theta-band coherence divided by the 0–40 Hz coherence), which is equal to 1 when there is no bias. Theta indices were highest for PYR during PV activation ($p < 0.05$, Kruskal-Wallis test corrected for multiple comparisons; Figure 2D). Theta-band entrainment was similar in CA1 and neocortical PYR (Figure 2D, insets).

Theta-band-limited discharge of PYR upon PV neuron activation can occur for at least two reasons. First, at high frequencies, the high density of spikes emitted by PV cells can tonically suppress their targets, whereas at lower frequencies PYR can still fire in longer windows devoid of strong PV activity, creating in effect a low-pass filter. This scenario is compatible with the frequency filtering properties of inhibitory synapses (Thomson et al., 2002; Markram et al., 2004). Second, active properties of pyramidal cells (Hu et al., 2002; Stuart et al., 2007) may induce time-locked rebound spiking upon recovery from inhibition (Llinás and Jahnsen, 1982; Cobb et al., 1995) of specific duration, creating in effect a band-pass filter. The finding that, on average, pyramidal cells were less suppressed by PV activation at low frequencies ($p < 0.001$, Kruskal-Wallis test; Figure 3Aa, bottom) is compatible with the first possibility. To examine the second possibility, we quantified the time-locking effect of PV photostimulation by calculating spiking gain (firing rate during chirp photostimulation, divided by baseline rate) as a function of frequency and phase (Figure 3Ab; Figure S3). While the mean firing rate of PYR was decreased by the chirp pattern at all phases and frequencies (Figure 3Aa), within the theta frequency band there was excess spiking at the stimulus trough, compared to control

periods ($p < 0.05$, Bonferroni-corrected permutation test; Figure 3Bb). Overall, 50/110 (45%) of the light-modulated PYR rebounded at the chirp pattern theta trough, with a median gain of 3.2 (range, 1.2–25; Figure 3Bc). The proportions and effect sizes were similar among neocortical and CA1 PYR ($p = 0.97$, χ^2 test; and $p = 0.91$, Mann-Whitney U test; Figure 3Bc; Figure S3). Thus, during PV activation with a chirp pattern, excess PYR spiking occurred at the trough of the theta band of the chirp stimulus.

Theta-Band Spiking Resonance Depends on the Inhibitory Pattern

To determine whether the frequency resonance of individual pyramidal cells depends on theta-frequency periodic inhibition by the PV cells, we compared the response to chirp and filtered white noise (WN; generated by convolving uncorrelated WN with a 3 ms exponential; Figure 4Aa) stimuli in a subset of cells (249 and 341 units in four CaMKII and eight PV mice, respectively; Figure 4B). Many units showed a visible time-locking to the WN pattern (Figure 4A; Mainen and Sejnowski, 1995), yet theta resonance of PYR spiking was not produced (Figure 4B). During CaMKII WN stimulation, only 10/206 (4.9%) of the PYR were modulated at some frequency ($p < 0.05$, permutation test; Figure 4B, top left). This low fraction was not due to ineffective stimulation, because the overall spiking rate (gain) was increased during both chirp and WN stimulation (Figure 4B, bottom left). A large fraction of interneurons was frequency-modulated in some band (for example, PV WN stimulation, 18/70 INT, 26%; Figure 4B, top left). Despite strong activation of PV neurons

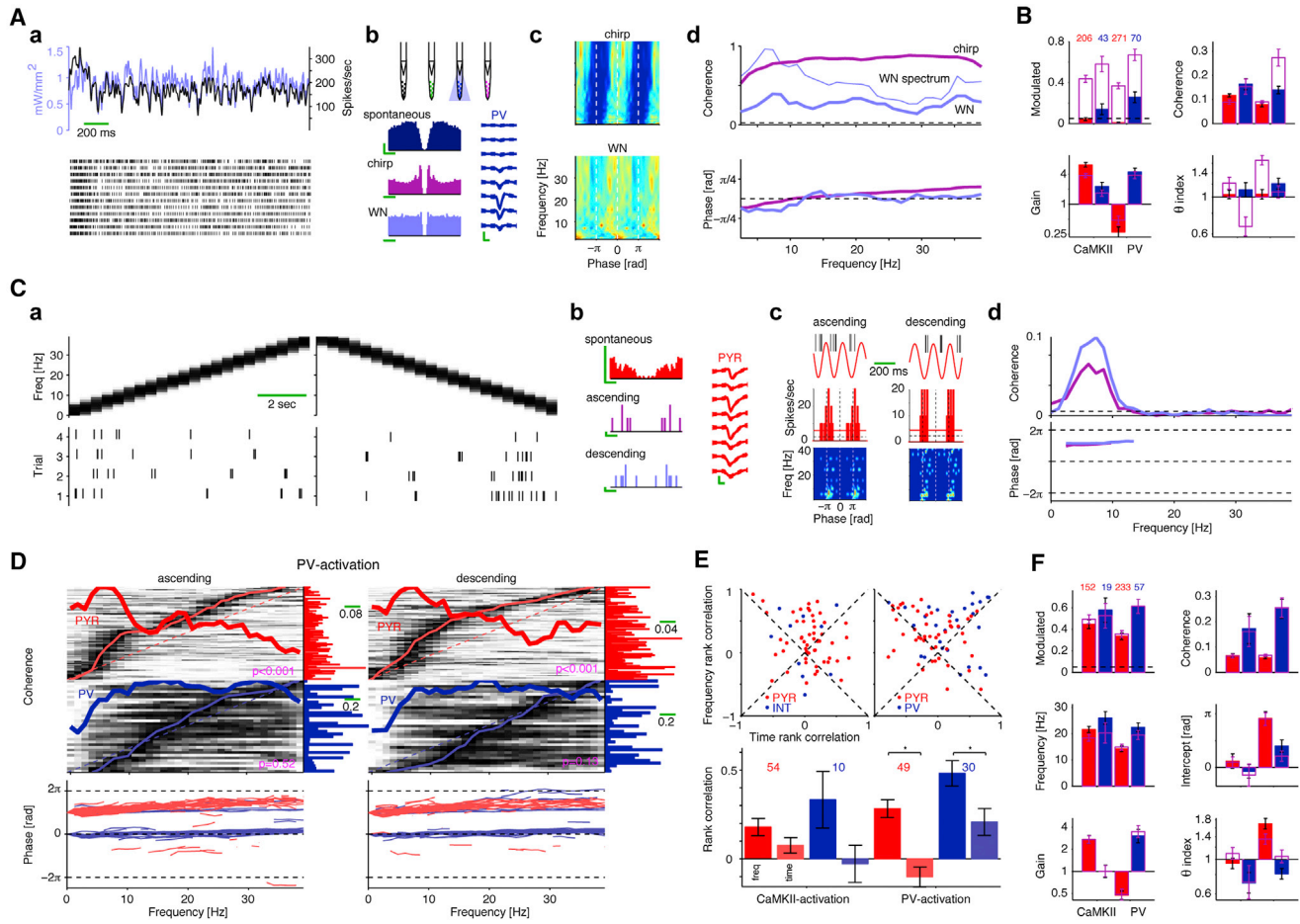


Figure 4. Inhibition-Induced PYR Spiking Depends on Inhibition Pattern

(A) WN stimulation of PV cells induces precisely timed PV spiking (CA1 region). (Aa) Stimulation pattern (light blue), and light-driven histogram of spiking (black overlay, rank correlation: 0.71) during 12 trials. Individual trials are shown at the bottom (black ticks). (Ab) Auto-correlation histograms during no-light control (spontaneous activity), chirp, and WN stimulation. Right, waveforms of the PV unit recorded at the eight recording sites. (Ac) Spiking frequency-phase maps as in Figure 3Ab (color scales: chirp, 0–460 spikes/sec; WN, 0–91.6 spikes/s). (Ad) Coherence and phase during the two photostimulation patterns. Note similar shapes of the coherence and spectrum of the input signal (superimposed WN spectrum).

(B) Full bars and purple bars show fraction of significantly modulated units during WN and chirp stimulation, respectively. Gain, coherence, and theta index are shown only for cells frequency modulated ($p < 0.05$, permutation test) by either pattern. PYR theta index is diminished during WN stimulation of PV cells.

(C) Spiking of a neocortical PYR during ascending (0–40 Hz) and descending (40–0 Hz) chirps (interleaved trials; Ca). Spiking is limited to the theta band in both cases. (Cb) Autocorrelation histograms. (Cc) Spiking histograms. Both patterns induce excess spiking during theta-band troughs (rebound). (Cd) Coherence and phase.

(D) Coherence and phase of light-modulated ($p < 0.05$) units tested with ascending- and descending-chirp patterns (PV-activation only). Phase is plotted only at frequencies for which coherence is significant. PYR spiking is predominantly at theta troughs regardless of chirp direction. Magenta numbers, Kolmogorov-Smirnov test (uniform null).

(E) Frequency-correlation (the rank correlation between the spiking coherence during ascending and descending chirps) versus the time-correlation (between the ascending chirp coherence and the temporally reversed descending coherence) for CaMKII (left) and PV (right) animals. Bottom, rank correlations for CaMKII and PV mice. $*p < 0.05$, Wilcoxon's paired signed rank test. Correlation with instantaneous chirp frequency is consistently larger than that with time.

(F) Statistics for the ascending (hollow purple bars) and descending (full bars) chirps. Note similar activity induced by the two patterns. (E) and (F) include only doubly modulated cells. For spiking gain maps and an equivalent presentation during CaMKII activation, see Figure S4.

(Figure 4B), the WN-induced inhibition did not induce phase-locked spiking in PYR because only 0.7% (2/271) PYR were significantly frequency modulated. This again was not due to inefficient suppression because WN-induced PYR spiking gains were similar, on a cell-by-cell basis, to chirp-induced suppression (rank correlation between spiking gains of 100 PYR modulated by either stimulus was 0.58; $p < 0.001$, permutation test).

In fact, WN pattern PV activation suppressed spiking more strongly than the chirp pattern (PYR gain during chirp: 0.49 ± 0.09 , and WN: 0.28 ± 0.07 ; $n = 100$ PYR; $p < 0.001$, U test; Figure 4B, bottom left). The lack of theta-band PYR spiking was not due to impaired spike following the stimulus either. PV cells followed the WN stimulus no less precisely than the chirp (mean \pm SEM phase slope during chirp: 0.05 ± 0.02 rad/Hz;

WN: -0.008 ± 0.009 ; $p = 0.02$, U test). Yet, PYR theta-band preference was absent during WN pattern PV activation (Figure 4B, bottom right). Thus, while WN PV activation was effective in directly inducing frequency-modulated PV spiking and indirectly suppressing PYR spiking, it was ineffective in inducing theta-band PYR spiking, suggesting that periodic inhibition is critical for spiking resonance.

In principle, part of the frequency preference of individual cells could result from slow adaptation (due to e.g., ChR2 dynamics, cellular adaptation, and/or calcium buildup). To examine this possibility, we tested a subset of units with both ascending (0–40 Hz) and descending (40–0 Hz) chirps (Figure 4C). Of 171 and 290 units tested under both conditions in three CaMKII and seven PV animals, 64 and 79 (37% and 27%) were light-modulated during both patterns (Figure 4DF; Figure S4). A few units showed temporal adaptation, while most maintained a similar frequency preference regardless of the chirp slope (Figure 4C). To quantify the frequency/time preference of individual units, we computed, for each cell, two rank correlation coefficients (“frequency correlation” and “time correlation”) between the coherences under the two conditions. For a pure frequency-dependent unit, the coherences during ascending and descending chirps should be identical, and the rank correlation between them (“frequency correlation”) is 1. In contrast, for a pure time-dependent unit, the coherences should be mirror images (assuming phase is preserved) and thus the rank correlation between the ascending chirp coherence and the reversed descending chirp coherence is 1. The mean \pm SEM frequency correlation was 0.19 ± 0.04 and 0.32 ± 0.04 for CaMKII and PV animals, respectively ($p < 0.001$ for both, permutation test with a zero correlation null), whereas the time correlation was 0.054 ± 0.04 and 0.02 ± 0.05 ($p = 0.02$ and $p = 0.6$; Figure 4E). Similar results were obtained when using linear or nonlinear models to explicitly predict coherence from time and frequency (Figure S4D). Population spiking properties were similar during ascending and descending chirp stimulation (Figure 4F). Similar to ascending chirp-pattern photostimulation (Figure 2), PYR displayed phase locking to chirp theta troughs and theta-band preference during descending chirp PV activation (Figure 4F; Figure S4A). In summary, resonant spiking of PYR upon PV activation does not result from adaptation processes, and a rhythmic pattern of inhibition is required for inhibition-induced resonant PYR spiking.

Spiking Resonance of Pyramidal Cells Depends on Inhibition Magnitude

If PYR spiking is actively induced during periodic inhibition, it should display a dependence on the magnitude of the inhibition. Because inhibition effects are more difficult to observe extracellularly in the absence of spiking, PYR spiking resonance may also depend on the baseline firing rate. During PV chirp-pattern activation, frequency-independent PYR spiking gain was negatively correlated with baseline rate (rank correlation, -0.31 ; $n = 110$ PYR; $p < 0.001$, permutation test; Figure S5A), presumably due to a spiking rate ceiling effect. PYR with higher baseline rates were also more coherent with the PV chirp stimulus (rank correlation, 0.31 ; $p = 0.003$; Figure S5B). This increased coherence may simply be a floor effect because silent cells cannot be sup-

pressed further. Finally, PYR preferred frequency was negatively correlated with baseline rate (rank correlation, -0.22 ; $p = 0.02$; Figure S5B).

To determine whether the frequency preference of individual units depends on the magnitude of the inhibitory drive, a subset of units was tested with multiple light intensities (167 and 329 units tested in four CaMKII and eight PV animals; Figure 5A). During PV activation, coherence between PV spikes and the chirp pattern in the theta band increased monotonously with light intensity (mean \pm SEM theta-band coherence: from 0.14 ± 0.03 to 0.22 ± 0.03 , $n = 19$ and 47 PV cells tested at one-fourth and at the optimal DC intensity). This was also reflected in a monotonous increase of the PYR tendency to spike predominantly at theta-band chirp frequency (theta index rank correlation with intensity was 0.17 ; $p = 0.04$; Figure 5B). In contrast, the frequency preference of neither PV during PV activation (Figure 5B) nor of PYR and INT during CaMKII activation (Figure S5D) varied consistently with light intensity. Thus, PYR subthreshold resonance was not communicated to the spiking regime even at low levels of CaMKII activation; instead, PYR spiking resonance increased with the level of PV activation (inhibition).

To determine the dependence of PYR resonant spiking on the actual local inhibitory drive, we computed, for each PYR, the theta peak spiking gain of the INT that was recorded simultaneously on the same shank (theta, 4–11 Hz; trough, four $\pi/10$ radian bins). For the purpose of this analysis, a single light intensity was used for each unit (the “optimal” DC intensity, Figure 1C). Of 342 PYR recorded during PV chirp activation, 272 (80%) were recorded with a same-shank INT. Of those PYR, 88 were significantly modulated ($p < 0.05$ permutation test). Local INT theta peak gain predicted chirp-spiking coherence in concurrently recorded PYR: the rank correlation was 0.3 for light-modulated PYR ($p < 0.001$, permutation test) and 0.52 for all PYR ($p < 0.001$; Figure S5E). With increased INT theta peak gain, PYR theta-band coherence increased and the theta phase of PYR spiking became less variable, as demonstrated by the increasing population circular resultant length (Figure 5C). Moreover, when the local inhibitory drive increased, PYR preferred frequency decreased and was closer to theta (Figure 5C; Figure S5E). Thus, theta-resonant PYR spiking depends on the effective magnitude of local inhibition.

Spiking Phases during Chirp Inhibition and Spontaneous Theta State Are Similar

To understand the interaction between native network connectivity and light-induced spiking resonance, we quantified the effect of chirp pattern activation on units recorded by nonlocal shanks. During single-shank chirp pattern PV activation, nonlocal units were weakly activated or not activated, similar to DC pulses (Figure 1C) and confirming previous demonstrations of local activation by the light cone (Stark et al., 2012). Yet, when nonlocal INT were frequency modulated, they showed a different pattern of activity compared to the local, directly activated PV neurons. For instance, during chirp-pattern PV activation on shank 2 of the CA1 circuit shown in Figure 6Aa, a PV recorded on shank 4 (400 μm away; Figure 6Ab, top right) spiked at the opposite phase of the chirp pattern and in a narrow frequency band. The same PV cell spiked at multiple frequencies

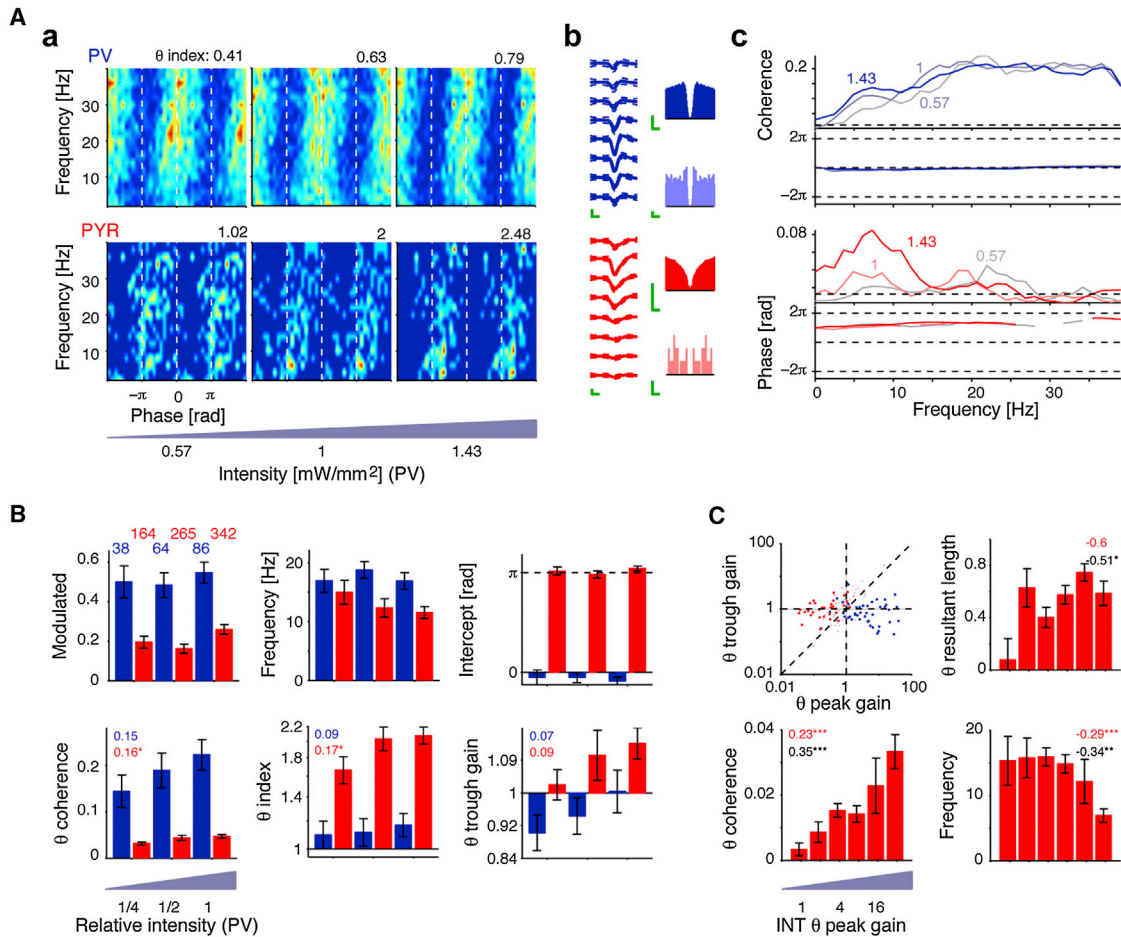


Figure 5. Inhibition-Induced PYR Spiking Depends on Magnitude of Inhibitory Drive

(A) PYR spiking is confined to theta troughs by increased inhibition. Two neocortical units, recorded from the same shank, were stimulated with a chirp pattern at three intensities (five repetitions/intensity). (Aa) Spiking frequency-phase maps for the PV interneuron (top; color scale, gain 0–7) and PYR (bottom; 0–2.5). (Ab) Spike waveforms and auto-correlation histograms for the two cells during evoked (bottom) and no-light (top) conditions. (Ac) Coherence and phase plots at different light intensities.

(B) Statistics for all units tested at multiple intensities during PV chirp-pattern activation. Relative intensity value of 1 corresponds to the “optimal” DC intensity (mean, 1.1 mW/mm² at the center of the illuminated shank; see Figure 1C). Neuron numbers and rank correlations for INT/PYR are shown in blue/red; */**/**p < 0.05/0.01/0.005, permutation test. PYR theta-band spiking is more prominent with increased intensity.

(C) PV interneuron theta peak gain predicts PYR theta-band coherence, phase, and specificity. Top left, During PV stimulation, spiking gain at the theta trough is higher than that at peak for PYR (p < 0.001, U test; red, n = 110 light-modulated cells; light red, not significantly modulated) but the inverse applies to PV interneurons (p < 0.001, n = 52; blue). Bar graphs show spiking properties of PYR during PV activation versus theta peak gain of INT recorded on the same shank. Rank correlations for significantly light-modulated PYR (n = 88) and all PYR (272) are shown in red/black text. As the local inhibitory drive increases, PYR theta-band coherence increases, PYR peak frequency decreases, and theta phase of PYR spiking becomes less variable (increased resultant length). See also Figure S5.

and in phase with the locally applied (shank 4) chirp (Figure 6Ab, bottom right). Thus, in contrast to local PV cells, which tended to spike around the chirp theta peak, nonlocal INT spiked increasingly closer to the chirp trough with increasing distance from the light source (circular-linear correlation: 0.45, p < 0.01, χ^2 test; mean \pm SEM of INT 400 μ m away from the illuminated shank: $(\pi - 0.16) \pm 0.6$ radians; Figure 6Ac). The PYR spiking phase did not vary with distance. Similar results were observed for neocortical cells (Figure S6A). Thus, nonlocal INT (possibly including PV and other types of INT) were inhibited by the local, light-activated PV neurons and/or activated by rebounding PYR.

During CaMKII activation, PYRs are subjected to two driving forces: direct light-induced spiking around the chirp peak, and indirect inhibition-mediated spiking around the chirp trough. While for locally recorded PYR, the second drive is overshadowed (Figure 2C, left), nonlocal PYR could spike after the CaMKII-driven chirp trough (circular-linear correlation: neocortex: 0.43, p < 0.05, χ^2 test; CA1: 0.24, p = 0.12; Figure S6B), consistent with the lack of direct light effect (Figure 1C, left) and network-mediated resonance.

To determine the relationship between light-generated, inhibition-induced spiking and spontaneous theta-band spiking

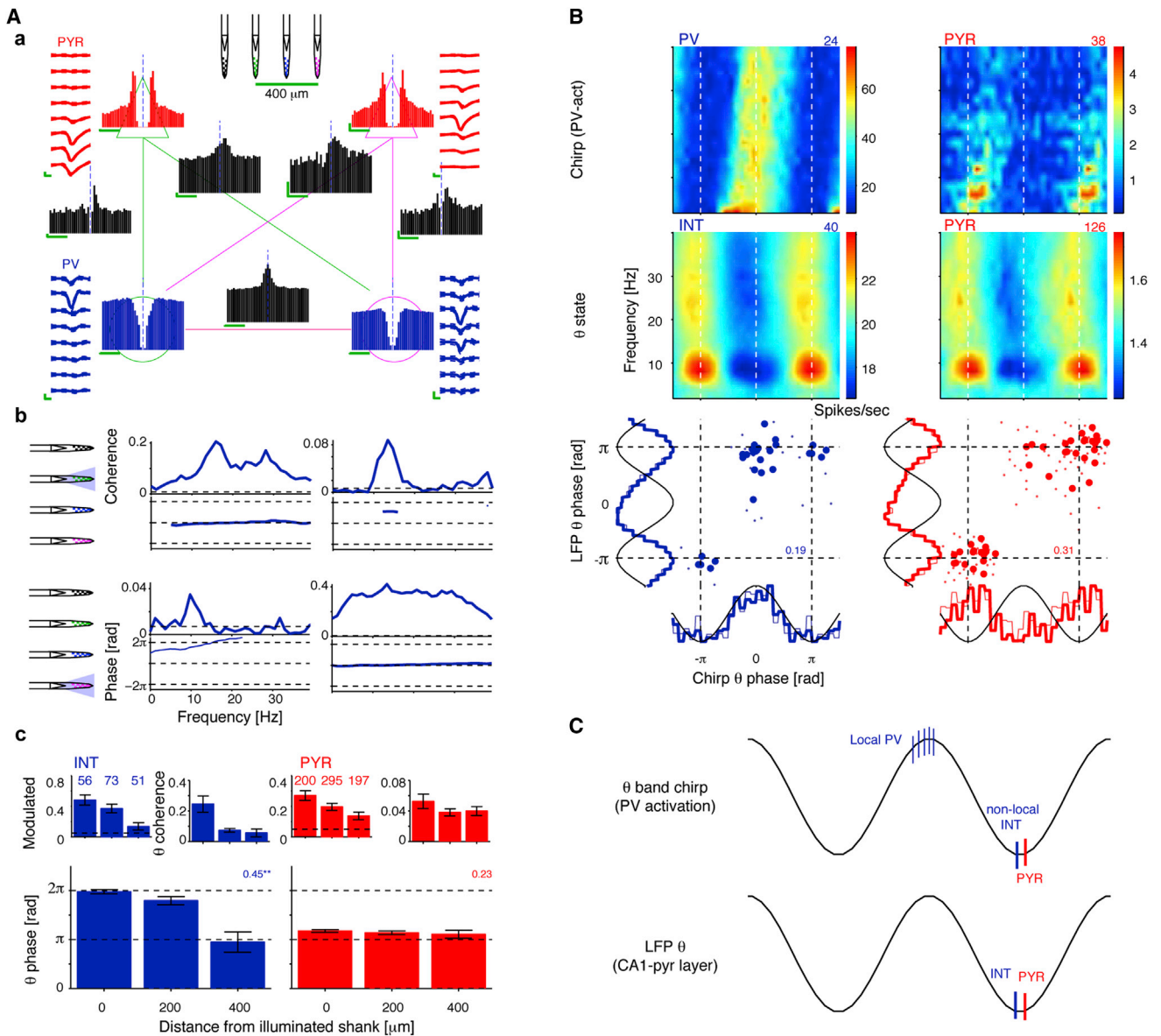


Figure 6. Phase Preference of Neuron Spikes during Induced Firing and LFP Theta Oscillations

(A) Nonlocal INT tend to spike at the trough of theta-band chirp pattern PV activation. (Aa) PYR-PV network recorded in CA1. One PYR and one PV are shown for each of two shanks, 400 μm apart. Auto- and cross-correlation histograms (calibration: 10 ms, 50 coincident counts) during spontaneous spiking (no-light condition) indicate monosynaptic connectivity of the same-shank PYR-PV pairs, zero-lag synchronization between the PV pair (on shanks 2 and 4), and time-shifted temporal correlation between cross-shank PYR-PV pairs. (Ab) Top: during chirp-pattern PV activation on shank 2, the local PV spikes in-phase with the chirp, whereas the nonlocal PV spikes anti-phase; the inverse occurs during PV activation on shank 4 (bottom). (Ac) During PV activation in CA1, PV recorded on the illuminated shank spike at peak of theta-band light stimulation whereas nonlocal INT tend to spike around the trough. PYR emit spikes near the trough. Circular-linear correlation coefficients are shown; ** $p < 0.01$, χ^2 test.

(B) Top: spiking frequency-phase maps of CA1 units during chirp-pattern PV activation. Only light-modulated units are included ($p < 0.05$, permutation test). Middle panels, spiking gain maps of CA1 units during LFP theta; only theta-band modulated units are included ($p < 0.05$, Rayleigh test). Bottom: phases for cells modulated by the chirp in the theta band and by LFP theta oscillations (both states: 24 PV, blue; 24 PYR, red; light dots, cells significantly modulated by either chirp or LFP theta). Circular-circular correlation coefficients are shown. Marginals show the mean firing rate (scaled 0–1 for each unit) during the two states (thin lines show marginals for cells modulated only in one state).

(C) Diagram summarizing the spiking phases of CA1 neurons during LFP theta (bottom) and during theta-band chirp-pattern PV-activation (top). During theta-band PV activation, locally driven PV cells follow the drive closely. Nonlocal cells spike at the opposite phase of the light-driven PV spikes.

See also Figure S6.

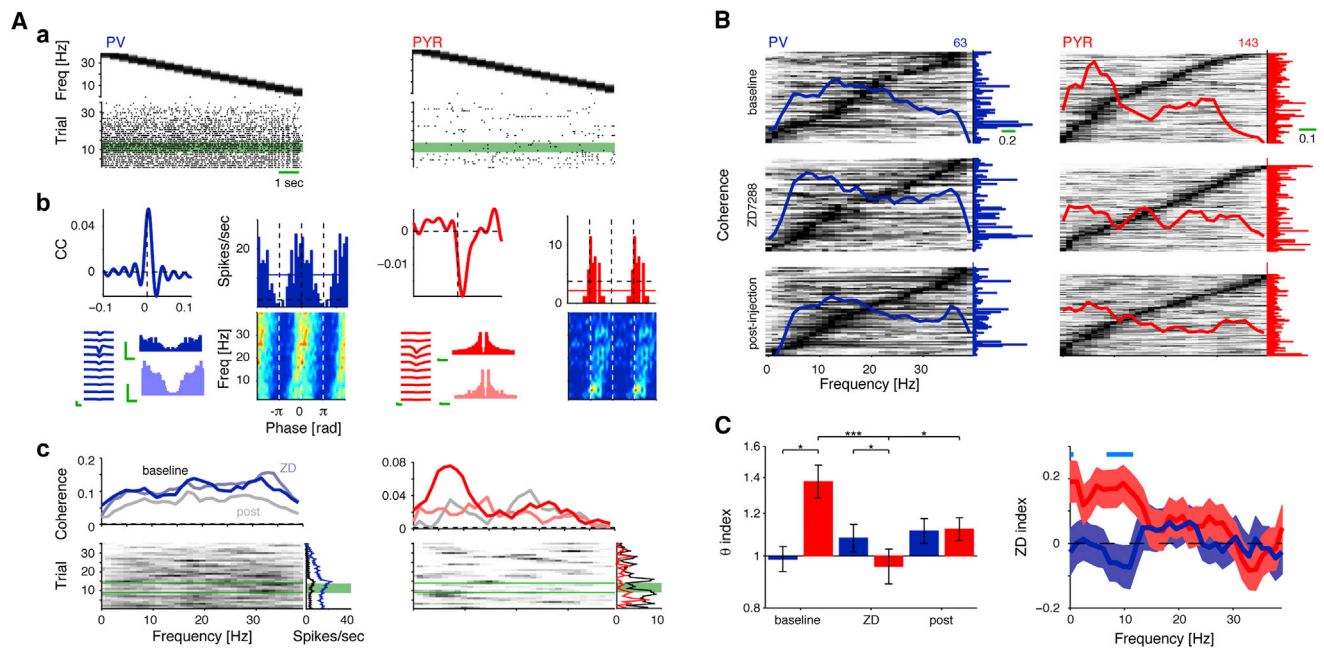


Figure 7. Theta-Band Rebound Spiking Is I_h Dependent

(A) Spiking of a CA1 PV (Aa, left) and PYR (right) recorded from the same diode-probe shank during 35 consecutive descending chirps (40–0 Hz; peak intensity, ~ 1 mW/mm²). An I_h blocker (ZD7288, 200 nM, 0.1 M) was infused into the CA1 radiatum/lacunosum-moleculare after the eighth chirp (shaded green region). (Ab) Spiking statistics before the injection. PV spiking exhibits theta-band resonance. (Ac) Bottom right, mean firing rate during (color) and surrounding (black) each chirp. While PV spiking is consistently driven by the chirp pattern (coherence by epochs/single-trials at top/bottom), PYR firing rate and theta-band coherence are diminished upon the infusion.

(B) ZD7288 attenuates theta-frequency resonance in PYR ($n = 5$ PV::ChR2 mice). Before ZD7288 injection, PYRs spike predominantly at the chirp-pattern theta band, whereas PVs spike uniformly at all frequencies. During I_h blockade, the frequency preference of PYR, but not of PV, changes and is no longer predominant in the theta band.

(C) Theta-band specificity of I_h -blockade. Left, Theta index of PYR is significantly reduced by the drug. Right, ZD-index (difference between control and drug coherence, divided by the sum) has high specificity for PYR during theta-band PV stimulation (blue bar, frequency bins for which PYR and PV indices differ; $p < 0.05$, Bonferroni-corrected U test).

See also Figure S7.

activity, we examined CA1 neurons during both chirp-pattern PV activation and spontaneous theta state (43 INT and 186 PYR recorded from six PV animals). As shown above, during chirp pattern PV activation in CA1, individual locally recorded PV cells spiked consistently at the chirp theta peak, whereas PYR emitted rebound spikes at theta trough (Figure 6B, top). In contrast, during behaviors associated with theta oscillations, both INT (40/43, 93%) and PYR (126/186, 67%) tend to spike near the trough of the locally recorded theta LFP (Figure 6B, center; Csicsvari et al., 1999). The spiking phase of individual PYR during spontaneous LFP theta and during the theta band of chirp pattern PV activation was similar, both at the population level (LFP theta mean \pm SEM phase, $(\pi - 0.07) \pm 0.17$ radians, $n = 126$; chirp phase, $(\pi + 0.19) \pm 0.26$ radians, $n = 38$; $p = 0.37$, permutation test) and at the single-cell level (circular-circular correlation, 0.31; mean \pm SEM phase difference, 0.14 ± 0.28 radians; $n = 24$ PYR, theta-modulated during both states; Figure 6B, bottom). Thus, during chirp pattern PV activation, both (local and nonlocal) PYR and (nonlocal) INT spiked near the stimulus trough, similar to the phase relationship during spontaneous theta oscillations, suggesting that similar mechanisms may un-

derlie the generation of PYR spiking during the two conditions (Figure 6C).

Theta-Band Spiking Resonance Depends on I_h Currents

A potential mechanism for the rebound spiking of CA1 PYR during theta-band inhibition is the activation of I_h conductance (Hu et al., 2002, Zemankovics et al., 2010). To test the hypothesized role of I_h , we infused a specific HCN1 channel blocker (ZD7288; Gasparini and DiFrancesco, 1997; Hu et al., 2002) into the CA1 radiatum/lacunosum-moleculare of urethane-anesthetized PV::ChR2 mice ($n = 5$) during chirp pattern photostimulation. Before to I_h blockade, theta-band spiking resonance could be induced in CA1 PYR cells (Figure 7A). Eighty-two percent (143/175) CA1 PYR cells and 94% (63/67) PV/INT were modulated by the chirp pattern ($p < 0.05$, permutation test). Similarly to the observations in the freely moving animals, during chirp-pattern activation of PV neurons, PYR spiked predominantly during stimulus troughs (linear phase model: $\Phi(f) = (\pi + 0.12) + 0.06f$; $R^2 = 0.87$) of the theta band (peak frequency, 9.8 ± 0.9 Hz; $p < 0.001$, Kolmogorov-Smirnov test comparing to a uniform distribution; Figure 7B, top). PV spiking was near

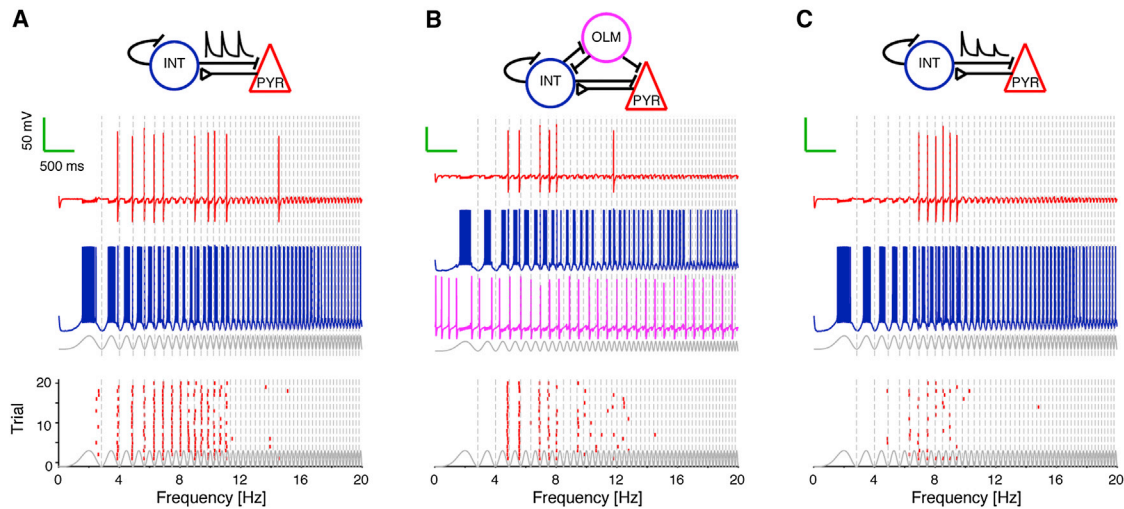


Figure 8. Model of Theta-Resonance Induced by Feedforward Inhibition

(A) A minimal network of a reciprocally connected PYR and INT (mimicking PV basket interneuron) was simulated and the INT was stimulated using the same chirp pattern used in the extracellular experiments. During stimulation, the PYR exhibited I_h -dependent postinhibitory spiking around the stimulus troughs (vertical dashed lines) at low frequencies.

(B) Addition of a timing mechanism, implemented here by an additional inhibitory interneuron (OLM cell), sharpens band-limited spiking. During low-frequency INT stimulation, the OLM cell was inhibited by the INT and released from inhibition “just in time” to inhibit PYR and prevent postinhibitory rebound during the high stimulus phase, in effect creating a PYR spiking band-pass filter. OLM cells are still active during the theta band. However, the combined effect of this inhibition and the OLM intrinsic properties, in particular I_h , generates a spiking frequency that does not interfere with PYR spiking.

(C) A similar pattern was obtained in the PYR-INT model by including synaptic depression of the inhibitory synapses on the PYR. Following intense presynaptic INT spiking, the inhibitory synapses on the PYR are less activated, so the hyperpolarization drive to I_h activation is reduced. Synaptic depression is more effective at lower input frequencies where the presynaptic input spiking is higher. Thus, at low stimulation frequencies, postinhibitory rebound spiking is not generated, resulting in theta-range resonant spiking.

zero-phase ($\Phi(f) = -0.06 + 0.04f$; $R^2 = 0.85$) and wide band (peak frequency, 17 ± 1.4 Hz; $p = 0.15$, Kolmogorov-Smirnov test).

Following ZD7288 infusion, local field activity and PYR spiking rates were slightly reduced (LFP: $p < 0.05$, Bonferroni-corrected paired t test; Figure S7A; PYR spiking: $p = 0.011$, Wilcoxon’s paired signed-rank test; Figure S7B), but synaptic transmission was maintained as PV activation consistently silenced PYR spiking (Figure S7C). In contrast, during and after I_h blocker infusion, theta-band preference of PYR spiking was abolished at the population ($p = 0.014$, U test comparing peak frequencies during control and drug effect periods; PV, $p = 0.74$; Figures 7A and 7B) and at the single-unit level ($p < 0.001$, Wilcoxon’s paired signed rank test comparing theta indices during control and drug-effect periods; PV, $p = 0.22$; Figure 7C, left). To further quantify the frequency-specificity of the drug effect for each unit, a “ZD-index” was computed (Figure 7C, right), defined as the difference between the control and drug effect coherence divided by the sum. This measure was selectively high for PYR at theta-band frequency ($p < 0.01$, Bonferroni-corrected Kolmogorov-Smirnov test). These findings suggest a direct involvement of HCN1 channels in inhibition-induced theta-band PYR spiking.

The pharmacological experiments established the requirement of I_h for theta-band spiking resonance but not its sufficiency. To investigate whether I_h alone is sufficient, we constructed a biophysical model of mutually connected PYR and INT with active currents driven by a chirp pattern current to the INT. When the PYR model included I_h , INT activation in

the low-frequency range induced rebound PYR spiking (Figure 8A). However, this range included sub-theta frequencies. Theta-band spiking regime resonance was especially robust when the model included a timing mechanism that prevented the generation of action potentials at low frequencies, implemented by either network-mediated timed inhibition (OLM cell; Rotstein et al., 2005; Figure 8B) or synaptic depression of the inhibitory synapses (Thomson et al., 2002; Markram et al., 2004; Pouille and Scanziani, 2004) on PYR (Figure 8C).

DISCUSSION

Using large-scale extracellular recordings and optogenetics in freely behaving mice, we showed that wide-band periodic but not random noise activation of PV interneurons induces theta frequency-favored spiking in hippocampal and neocortical pyramidal cells accompanied by postinhibitory rebound spiking. Pharmacological blockade of I_h abolished the suprathreshold (spiking) resonance. These findings demonstrate that spike transmission in pyramidal cells is enhanced in the theta band and that this effect is due to an interaction between intrinsic cellular properties and network mechanisms.

Previous in vitro work described theta-band subthreshold resonance in cortical principal neurons using an intracellularly applied sinusoidal pattern (Leung and Yu, 1998; Dickson et al., 2000; Hu et al., 2002, 2007, 2009; Ulrich, 2002; Peters et al., 2005; Wang et al., 2006; Giacomo et al., 2007; Marcelin et al., 2009; Gastrein et al., 2011). In contrast, we observed

increased spiking probabilities at different chirp frequencies in different CA1 and neocortical pyramidal neurons, and an overall wide-band response. The *in vitro* tests typically examined resonance by intracellular current injection of a chirp pattern at a hyperpolarized membrane potential while synaptic activity was blocked pharmacologically. The difference between the *in vivo* and *in vitro* results can be explained by the presence of synaptic activity *in vivo* and/or the depolarizing effect of the light-induced chirp in our experiments. Because I_h is largely deactivated near spike threshold (Ulrich, 2002; Wang et al., 2006; Hu et al., 2009; Gastrein et al., 2011), lack of systematic theta resonance of directly activated pyramidal cells in our experiments may be attributed to the direct depolarizing effect of photoactivation. In addition, the membrane resistance of neurons in a waking animal is much lower than that *in vitro* due to high synaptic activity (Destexhe et al., 2003), which may increase the ability of neurons to spike at higher input frequencies.

We achieved chirp-pattern hyperpolarization in PYR indirectly by optogenetic activation of the PV cells. Individual locally recorded PV cells reliably followed the alternating light patterns up to 40 Hz but showed no particular frequency preference, consistent with the lack of I_h in basket cells (Zemankovics et al., 2010). Yet, despite the wide-band spike following of PV interneurons, the indirectly inhibited pyramidal cells exhibited robust spike transmission in the theta band. Although several mechanisms might account for the theta-band spiking resonance (Hu et al., 2002), our experiments suggest that to a large part, the effect is mediated by the activation of HCN channels in pyramidal cells, because pharmacological blockade of HCN channels largely abolished theta-band spiking resonance.

Light-evoked wide-band spiking of PV neurons induced an overall inhibition of the concurrently monitored pyramidal cells. However, in the theta band, the spiking rate was comparable with the baseline activity and, in many neocortical and hippocampal pyramidal cells, a significant rate increase at the trough of the theta-band light stimulus was observed. Such frequency-dependent enhancement of spiking provides further support of an HCN-mediated mechanism, since posthyperpolarization rebound spiking has been documented in several types of neurons with high density of HCN channels (Linás and Yarom, 1986; Marder and Calabrese, 1996; McCormick and Bal, 1997; Maccaferri and McBain, 1996; Steriade et al., 1993). The lack of frequency band preference and excess spiking upon WN stimulation is also consistent with the rhythmogenic properties of HCN channels (McCormick and Bal, 1997; Lüthi and McCormick, 1998). Whereas previous *in vitro* and the present *in vivo* experiments provide strong support for a critical role of HCN channels in theta-band resonance and excess rebound spiking of pyramidal cells following periodic inhibition, additional mechanisms (Figures 8B and 8C) may sharpen PYR spiking resonance in the intact network.

Spiking resonance may contribute to entrainment of neocortical neurons by the hippocampus (Siapas et al., 2005; Sirota et al., 2008). Theta-band rhythmic output from the hippocampus/entorhinal cortex may bring about feed-forward excitation of fast-firing basket cells, and possibly other interneuron types, the inhibitory effects of which may be amplified by the theta-resonant spiking properties of layer 5 pyramidal cells. Such inter-

neuron-mediated amplification mechanisms may temporally align spatially widespread cortical assemblies via few axonal links. It is possible that the spiking resonance in the neocortex is also used to amplify other patterns that overlap in frequency with the theta band, such as alpha oscillations (Klimesch et al., 2007) and sleep spindles (Steriade et al., 1993).

The weak focal photostimulation affected an estimated 2–20 PV interneurons (depending on light intensity and cell density; Royer et al., 2012; Stark et al., 2012), and did not affect the frequency or phase of the global theta rhythm (Figures S6C and S6D). The light-activated local neurons continued to be under the control of native network mechanisms as well. How does this dual control of PV interneurons relate to the timing of cell assembly activity under physiological operations? During chirp-pattern photoactivation, local PV cells and PYR fired on opposite phases of the sinusoidal chirp pattern. In contrast, both putative fast-spiking basket cells and pyramidal cells in the unperturbed CA1 circuit fire, on average, near the trough of the local LFP theta cycle (Figure 6C; Csicsvari et al., 1999; Klausberger et al., 2003). Yet, grand averages do not correctly describe the dynamic relationship between pyramidal cells and perisomatic interneurons. During exploration, although the maximal number of action potentials is fired at the trough of theta in the middle of the place field (Dragoi and Buzsáki, 2006), the spikes of CA1 pyramidal cells undergo a systematic theta phase shift as an animal traverses the place field of the neuron (O'Keefe and Recce, 1993). At the same time, putative postsynaptic basket cells display a similar phase precession (Maurer et al., 2006; Geisler et al., 2007). A hypothesized function of this conjoined phase shift is that only a single cell assembly is active in a given phase space of the theta cycle, and that the phase-shifting basket cells suppress the competing assemblies (Maurer et al., 2006; Royer et al., 2012). Consequently, spikes of place cells and basket cells of the same assembly share the same theta phase, but spikes of basket interneurons driven by the currently dominant assembly and place cells of the competing assembly fire at the opposite phases of the theta waves (Maurer et al., 2006). The current results support such a mechanism.

In addition to spatial navigation, hippocampal neurons support episodic memory and can generate evolving cell assemblies underlying such operations even in the absence of environmental or bodily derived cues (Pastalkova et al., 2008; Itskov et al., 2011; MacDonald et al., 2011). We hypothesize that the rebound spikes, induced by release from PV interneuron-mediated inhibition, contribute to the initiation of runner-up assemblies. In this framework, PV interneurons of the currently active CA1 cell assembly spiking at the trough of the theta cycle suppress competing assemblies but, at the same time, may induce rebound spikes at the opposite phase of the theta cycle in the most strongly inhibited/competing neurons, which can become, in turn, a seed of activation for the upcoming assembly. While speculative, this hypothesis is compatible with all known observations on putative basket neurons (Klausberger and Somogyi, 2008) and their temporal relationship with pyramidal cells, including the present observations.

In summary, our experiments uncovered an inhibition-based component of theta-band spiking resonance, which may affect the frequency-dependence of spiking in the hippocampus and

neocortex. The circuit properties described herein enable preferential transmission of theta-frequency activity to target populations, postsynaptic to theta-oscillating interneurons, and may amplify theta-range spiking in local circuits.

EXPERIMENTAL PROCEDURES

Four CaMKII::ChR2 mice were used in this study: two wild-type (C57L/6J, Jackson Labs), injected with rAAV5/CaMKIIa-hChR2(h134R)-EYFP into cortex and hippocampus, PA, 1.6/ml 1.1 mm; and two transgenic Rosa-CAG-LSL-ChR2(h134R)-EYFP-WPRE; Ai-32, Allen Institute; Madisen et al., 2012; crossed with B6.Cg-Tg(Camk2a-cre)T29-1St/J, Jackson Labs. Eight PV::ChR2 mice (Ai-32 crossed with B6;129P2-Pvalb tm1(cre)Arbr/J, Jackson Labs) were used for chronic recordings and an additional five PV::ChR2 for acute experiments. For chronic experiments, animals were implanted with multishank diode probes (Stark et al., 2012) constructed by coupling 470 nm LEDs and/or 405 nm laser diodes to 50 μ m optical fibers and attaching each diode-fiber assembly to a single shank of commercially available silicon probes (NeuroNexus). Chronic recordings were carried out as the probe was moved gradually from neocortex to CA1; at each site, light stimulation (peak driving current, 60 mA; peak power: 470 nm: $35 \pm 7 \mu$ W; 405 nm: $231 \pm 62 \mu$ W) was applied by 50–70 ms pulses, linear chirps (0–40 Hz or 40–0 Hz, 10 s), and WN (filtered with a 3 ms exponential). Data were recorded with a 128 channel system (16 bit, 20 kHz; RC Electronics). For acute experiments, animals were anesthetized with urethane (1.5 g/kg) and an I_h blocker (ZD7288, Tocris; 0.1–1 M) was injected stereotactically into the CA1 radiatum/lacunosum-moleculare while concurrently recording from the CA1 pyramidal cell layer and applying linear chirps.

Spikes were isolated offline and sorted into single units automatically (Harris et al., 2000) followed by manual adjustment. Only well-isolated units (amplitude > 50 μ V; L-ratio < 0.05, Schmitzer-Torbert et al., 2005; ISI index < 0.2, Fee et al., 1996) were considered. Units were classified into putative PYR or INT based on short-latency features in the cross-correlation histograms (PYR/INT-tagging; Barthó et al., 2004), responses to brief light pulses (PV-tagging), or waveform features (Gaussian-mixture model-based classifier, trained by the cross-correlation and PV-tagging data). A total of 1,413 units were recorded (chronic animals); of those, 1,151 were classified ($p < 0.05$) as PYR, 240 as INT; 22 were unclassified (Figure S1). For each unit recorded during linear chirp stimulation, the multi-taper coherence and phase were estimated between the current driving the diode and the raw spike train (both digitized at 1,250 Hz). Significance was estimated by a permutation test (computing the coherence between the chirp pattern and spike trains selected at random from periods without light stimulation) corrected for multiple comparisons. Spiking maps as a function of frequency and phase were constructed by segmenting the chirp into discrete frequencies and assigning a frequency and phase to each spike, and the resulting count histograms were divided by the spontaneous spiking rate (in the lack of any light stimulation) to yield gain maps.

SUPPLEMENTAL INFORMATION

Supplemental Information includes Supplemental Experimental Procedures and seven figures and can be found with this article online at <http://dx.doi.org/10.1016/j.neuron.2013.09.033>.

AUTHOR CONTRIBUTIONS

E.S. designed the experiments; E.S. and R.E. constructed diode-probes; L.R. and S.F. maintained transgenic animals; L.R. performed histology; E.S., L.R., and R.E. performed experiments; E.S. analyzed data; E.S. and H.G.R. constructed models; and E.S. and G.B. wrote the paper.

ACKNOWLEDGMENTS

We thank Kenji Mizuseki and Anton Sirota for insightful comments and Karl Deisseroth for providing the rAAV5-CaMKII::ChR2 virus. This study was sup-

ported by NIH NS034994 (to G.B.), NIH MH54671 (to G.B.), NS074015 (to G.B.), the Rothschild Foundation (to E.S.), the Human Frontiers in Science Project LT-000346/2009-L (to E.S.), the Machiah Foundation (to E.S.), NSF DMS-0817241 (to H.G.R.), and DMS-1313861 (to H.G.R.).

Accepted: September 17, 2013

Published: December 4, 2013

REFERENCES

- Barthó, P., Hirase, H., Monconduit, L., Zugaro, M., Harris, K.D., and Buzsáki, G. (2004). Characterization of neocortical principal cells and interneurons by network interactions and extracellular features. *J. Neurophysiol.* 92, 600–608.
- Boyden, E.S., Zhang, F., Bamberg, E., Nagel, G., and Deisseroth, K. (2005). Millisecond-timescale, genetically targeted optical control of neural activity. *Nat. Neurosci.* 8, 1263–1268.
- Buzsáki, G. (2002). Theta oscillations in the hippocampus. *Neuron* 33, 325–340.
- Buzsáki, G., and Moser, E.I. (2013). Memory, navigation and theta rhythm in the hippocampal-entorhinal system. *Nat. Neurosci.* 16, 130–138.
- Cobb, S.R., Buhl, E.H., Halasy, K., Paulsen, O., and Somogyi, P. (1995). Synchronization of neuronal activity in hippocampus by individual GABAergic interneurons. *Nature* 378, 75–78.
- Csicsvari, J., Hirase, H., Czurkó, A., Mamiya, A., and Buzsáki, G. (1999). Oscillatory coupling of hippocampal pyramidal cells and interneurons in the behaving Rat. *J. Neurosci.* 19, 274–287.
- Destexhe, A., Rudolph, M., and Paré, D. (2003). The high-conductance state of neocortical neurons in vivo. *Nat. Rev. Neurosci.* 4, 739–751.
- Dickson, C.T., Magistretti, J., Shalinsky, M.H., Fransén, E., Hasselmo, M.E., and Alonso, A. (2000). Properties and role of $I(h)$ in the pacing of subthreshold oscillations in entorhinal cortex layer II neurons. *J. Neurophysiol.* 83, 2562–2579.
- Dragoi, G., and Buzsáki, G. (2006). Temporal encoding of place sequences by hippocampal cell assemblies. *Neuron* 50, 145–157.
- Erchova, I., Kreck, G., Heinemann, U., and Herz, A.V. (2004). Dynamics of rat entorhinal cortex layer II and III cells: characteristics of membrane potential resonance at rest predict oscillation properties near threshold. *J. Physiol.* 560, 89–110.
- Fee, M.S., Mitra, P.P., and Kleinfeld, D. (1996). Automatic sorting of multiple unit neuronal signals in the presence of anisotropic and non-Gaussian variability. *J. Neurosci. Methods* 69, 175–188.
- Gasparini, S., and DiFrancesco, D. (1997). Action of the hyperpolarization-activated current (I_h) blocker ZD 7288 in hippocampal CA1 neurons. *Pflugers Arch.* 435, 99–106.
- Gastrein, P., Campanac, E., Gassel, C., Cudmore, R.H., Bialowas, A., Carlier, E., Fronzaroli-Molinieres, L., Ankri, N., and Debanne, D. (2011). The role of hyperpolarization-activated cationic current in spike-time precision and intrinsic resonance in cortical neurons in vitro. *J. Physiol.* 589, 3753–3773.
- Geisler, C., Robbe, D., Zugaro, M., Sirota, A., and Buzsáki, G. (2007). Hippocampal place cell assemblies are speed-controlled oscillators. *Proc. Natl. Acad. Sci. USA* 104, 8149–8154.
- Giocomo, L.M., Zilli, E.A., Fransén, E., and Hasselmo, M.E. (2007). Temporal frequency of subthreshold oscillations scales with entorhinal grid cell field spacing. *Science* 315, 1719–1722.
- Harris, K.D., Henze, D.A., Csicsvari, J., Hirase, H., and Buzsáki, G. (2000). Accuracy of tetrode spike separation as determined by simultaneous intracellular and extracellular measurements. *J. Neurophysiol.* 84, 401–414.
- Haas, J.S., and White, J.A. (2002). Frequency selectivity of layer II stellate cells in the medial entorhinal cortex. *J. Neurophysiol.* 88, 2422–2429.

- Hu, H., Vervaeke, K., and Storm, J.F. (2002). Two forms of electrical resonance at theta frequencies, generated by M-current, h-current and persistent Na⁺ current in rat hippocampal pyramidal cells. *J. Physiol.* *545*, 783–805.
- Hu, H., Vervaeke, K., and Storm, J.F. (2007). M-channels (Kv7/KCNQ channels) that regulate synaptic integration, excitability, and spike pattern of CA1 pyramidal cells are located in the perisomatic region. *J. Neurosci.* *27*, 1853–1867.
- Hu, H., Vervaeke, K., Graham, L.J., and Storm, J.F. (2009). Complementary theta resonance filtering by two spatially segregated mechanisms in CA1 hippocampal pyramidal neurons. *J. Neurosci.* *29*, 14472–14483.
- Hutcheon, B., and Yarom, Y. (2000). Resonance, oscillation and the intrinsic frequency preferences of neurons. *Trends Neurosci.* *23*, 216–222.
- Itskov, V., Curto, C., Pastalkova, E., and Buzsáki, G. (2011). Cell assembly sequences arising from spike threshold adaptation keep track of time in the hippocampus. *J. Neurosci.* *31*, 2828–2834.
- Klausberger, T., and Somogyi, P. (2008). Neuronal diversity and temporal dynamics: the unity of hippocampal circuit operations. *Science* *321*, 53–57.
- Klausberger, T., Magill, P.J., Márton, L.F., Roberts, J.D., Cobden, P.M., Buzsáki, G., and Somogyi, P. (2003). Brain-state- and cell-type-specific firing of hippocampal interneurons in vivo. *Nature* *421*, 844–848.
- Klimesch, W., Sauseng, P., and Hanslmayr, S. (2007). EEG alpha oscillations: the inhibition-timing hypothesis. *Brain Res. Brain Res. Rev.* *53*, 63–88.
- Lengyel, M., Kwag, J., Paulsen, O., and Dayan, P. (2005). Matching storage and recall: hippocampal spike timing-dependent plasticity and phase response curves. *Nat. Neurosci.* *8*, 1677–1683.
- Leung, L.S., and Yu, H.W. (1998). Theta-frequency resonance in hippocampal CA1 neurons in vitro demonstrated by sinusoidal current injection. *J. Neurophysiol.* *79*, 1592–1596.
- Llinás, R., and Jahnsen, H. (1982). Electrophysiology of mammalian thalamic neurones in vitro. *Nature* *297*, 406–408.
- Llinás, R., and Yarom, Y. (1986). Oscillatory properties of guinea-pig inferior olivary neurones and their pharmacological modulation: an in vitro study. *J. Physiol.* *376*, 163–182.
- Lőrincz, A., Notomi, T., Tamás, G., Shigemoto, R., and Nusser, Z. (2002). Polarized and compartment-dependent distribution of HCN1 in pyramidal cell dendrites. *Nat. Neurosci.* *5*, 1185–1193.
- Lüthi, A., and McCormick, D.A. (1998). H-current: properties of a neuronal and network pacemaker. *Neuron* *21*, 9–12.
- Maccaferri, G., and McBain, C.J. (1996). The hyperpolarization-activated current (I_h) and its contribution to pacemaker activity in rat CA1 hippocampal stratum oriens-alveus interneurons. *J. Physiol.* *497*, 119–130.
- MacDonald, C.J., Lepage, K.Q., Eden, U.T., and Eichenbaum, H. (2011). Hippocampal “time cells” bridge the gap in memory for discontinuous events. *Neuron* *71*, 737–749.
- Madisen, L., Mao, T., Koch, H., Zhuo, J.M., Berenyi, A., Fujisawa, S., Hsu, Y.W., Garcia, A.J., 3rd, Gu, X., Zanella, S., et al. (2012). A toolbox of Cre-dependent optogenetic transgenic mice for light-induced activation and silencing. *Nat. Neurosci.* *15*, 793–802.
- Magee, J.C. (1998). Dendritic hyperpolarization-activated currents modify the integrative properties of hippocampal CA1 pyramidal neurons. *J. Neurosci.* *18*, 7613–7624.
- Mainen, Z.F., and Sejnowski, T.J. (1995). Reliability of spike timing in neocortical neurons. *Science* *268*, 1503–1506.
- Marcelin, B., Chauvière, L., Becker, A., Migliore, M., Esclapez, M., and Bernard, C. (2009). h channel-dependent deficit of theta oscillation resonance and phase shift in temporal lobe epilepsy. *Neurobiol. Dis.* *33*, 436–447.
- Marder, E., and Calabrese, R.L. (1996). Principles of rhythmic motor pattern generation. *Physiol. Rev.* *76*, 687–717.
- Markram, H., Toledo-Rodriguez, M., Wang, Y., Gupta, A., Silberberg, G., and Wu, C. (2004). Interneurons of the neocortical inhibitory system. *Nat. Rev. Neurosci.* *5*, 793–807.
- Maurer, A.P., Cowen, S.L., Burke, S.N., Barnes, C.A., and McNaughton, B.L. (2006). Phase precession in hippocampal interneurons showing strong functional coupling to individual pyramidal cells. *J. Neurosci.* *26*, 13485–13492.
- McCormick, D.A., and Bal, T. (1997). Sleep and arousal: thalamocortical mechanisms. *Annu. Rev. Neurosci.* *20*, 185–215.
- O’Keefe, J., and Recce, M.L. (1993). Phase relationship between hippocampal place units and the EEG theta rhythm. *Hippocampus* *3*, 317–330.
- Narayanan, R., and Johnston, D. (2008). The h channel mediates location dependence and plasticity of intrinsic phase response in rat hippocampal neurons. *J. Neurosci.* *28*, 5846–5860.
- Pastalkova, E., Itskov, V., Amarasingham, A., and Buzsáki, G. (2008). Internally generated cell assembly sequences in the rat hippocampus. *Science* *321*, 1322–1327.
- Peters, H.C., Hu, H., Pongs, O., Storm, J.F., and Isbrandt, D. (2005). Conditional transgenic suppression of M channels in mouse brain reveals functions in neuronal excitability, resonance and behavior. *Nat. Neurosci.* *8*, 51–60.
- Pike, F.G., Goddard, R.S., Suckling, J.M., Ganter, P., Kasthuri, N., and Paulsen, O. (2000). Distinct frequency preferences of different types of rat hippocampal neurones in response to oscillatory input currents. *J. Physiol.* *529*, 205–213.
- Pouille, F., and Scanziani, M. (2004). Routing of spike series by dynamic circuits in the hippocampus. *Nature* *429*, 717–723.
- Richardson, M.J., Brunel, N., and Hakim, V. (2003). From subthreshold to firing-rate resonance. *J. Neurophysiol.* *89*, 2538–2554.
- Robinson, R.B., and Siegelbaum, S.A. (2003). Hyperpolarization-activated cation currents: from molecules to physiological function. *Annu. Rev. Physiol.* *65*, 453–480.
- Rotstein, H.G., Pervouchine, D.D., Acker, C.D., Gillies, M.J., White, J.A., Buhl, E.H., Whittington, M.A., and Kopell, N. (2005). Slow and fast inhibition and an H-current interact to create a theta rhythm in a model of CA1 interneuron network. *J. Neurophysiol.* *94*, 1509–1518.
- Royer, S., Zemelman, B.V., Losonczy, A., Kim, J., Chance, F., Magee, J.C., and Buzsáki, G. (2012). Control of timing, rate and bursts of hippocampal place cells by dendritic and somatic inhibition. *Nat. Neurosci.* *15*, 769–775.
- Santoro, B., Chen, S., Luthi, A., Pavlidis, P., Shumyatsky, G.P., Tibbs, G.R., and Siegelbaum, S.A. (2000). Molecular and functional heterogeneity of hyperpolarization-activated pacemaker channels in the mouse CNS. *J. Neurosci.* *20*, 5264–5275.
- Schmitzer-Torbert, N., Jackson, J., Henze, D., Harris, K., and Redish, A.D. (2005). Quantitative measures of cluster quality for use in extracellular recordings. *Neuroscience* *131*, 1–11.
- Siapas, A.G., Lubenov, E.V., and Wilson, M.A. (2005). Prefrontal phase locking to hippocampal theta oscillations. *Neuron* *46*, 141–151.
- Sirota, A., Montgomery, S., Fujisawa, S., Isomura, Y., Zugaro, M., and Buzsáki, G. (2008). Entrainment of neocortical neurons and gamma oscillations by the hippocampal theta rhythm. *Neuron* *60*, 683–697.
- Stark, E., and Abeles, M. (2009). Unbiased estimation of precise temporal correlations between spike trains. *J. Neurosci. Methods* *179*, 90–100.
- Stark, E., Koos, T., and Buzsáki, G. (2012). Diode probes for spatiotemporal optical control of multiple neurons in freely moving animals. *J. Neurophysiol.* *108*, 349–363.
- Steriade, M., McCormick, D.A., and Sejnowski, T.J. (1993). Thalamocortical oscillations in the sleeping and aroused brain. *Science* *262*, 679–685.
- Stuart, G., and Spruston, N. (1998). Determinants of voltage attenuation in neocortical pyramidal neuron dendrites. *J. Neurosci.* *18*, 3501–3510.

- Stuart, G., Spruston, N., and Häusser, M. (2007). *Dendrites*. (New York: Oxford University Press).
- Thomson, A.M., Bannister, A.P., Mercer, A., and Morris, O.T. (2002). Target and temporal pattern selection at neocortical synapses. *Philos. Trans. R. Soc. Lond. B Biol. Sci.* *357*, 1781–1791.
- Ulrich, D. (2002). Dendritic resonance in rat neocortical pyramidal cells. *J. Neurophysiol.* *87*, 2753–2759.
- Wang, W.T., Wan, Y.H., Zhu, J.L., Lei, G.S., Wang, Y.Y., Zhang, P., and Hu, S.J. (2006). Theta-frequency membrane resonance and its ionic mechanisms in rat subicular pyramidal neurons. *Neuroscience* *140*, 45–55.
- Zemankovics, R., Káli, S., Paulsen, O., Freund, T.F., and Hájos, N. (2010). Differences in subthreshold resonance of hippocampal pyramidal cells and interneurons: the role of h-current and passive membrane characteristics. *J. Physiol.* *588*, 2109–2132.